THE JOURNAL OF PHYSICAL CHEMISTRY B

Article

pubs.acs.org/JPCB

Dicationic versus Monocationic Ionic Liquids: Distinctive Ionic Dynamics and Dynamical Heterogeneity

Tateki Ishida*,† and Hideaki Shirota*,‡

†Department of Theoretical and Computational Molecular Science, Institute for Molecular Science, 38 Nishigo-Naka, Myodaiji, Okazaki 444-8585, Japan

‡Department of Nanomaterial Science, Graduate School of Advanced Integration Science & Department of Chemistry, Faculty of Science, Chiba University, 1-33 Yayoi, Inage-ku, Chiba 263-8522, Japan

Supporting Information

ABSTRACT: The dynamical properties of a dicationic ionic liquid (IL), 1,6-bis(3-methylimidazolium-1-yl)hexane bis(trifluoromethylsulfonyl)amide ($[C_6(MIm)_2][NTf_2]_2$), compared to 1-methyl-3-propylimidazolium bis-(trifluoromethylsulfonyl)amide ($[C_3MIm][NTf_2]$), as its monocationic imidazolic counterpart, are studied by molecular dynamics simulations. We investigate relaxation processes of the polarizability anisotropy of the system and collective dynamics of both the ILs with mean-squared displacement (MSD), non-Gaussian parameter, and the intermediate scattering functions. The analyses of librational dynamics show that the difference of the Kerr spectra between the ILs could be mainly ascribed to the distinctive angular momentum of $[C_6(MIm)_2]^{2+}$ and $[C_3MIm]^+$ and related to the difference of relaxation behavior between $[C_6(MIm)_2]^{2+}$ and $[C_3MIm]^+$. Also, it is indicated that the librational dynamics of $[NTf_2]^-$ indicate a common resonance-type sharp peak that corresponds to an intermolecular motion coupled to the vibrational mode intrinsic to $[NTf_2]^-$. In addition, it is exhibited from the total X-ray structure factors calculated for both of the ILs that the low-k peak at 0.20 Å^{-1} appears for $[C_6(MIm)_2][NTf_2]_2$, while we do not see it for $[C_3MIm][NTf_2]$. We find that the contribution of the anion−cation and anion−anion correlations to the low-k peak is more significant than the cation−cation correlation. Therefore, it is suggested for $[C_6(MIm)_2][NTf_2]_2$ that dynamical heterogeneous behavior strongly correlates with structural variations or heterogeneity.

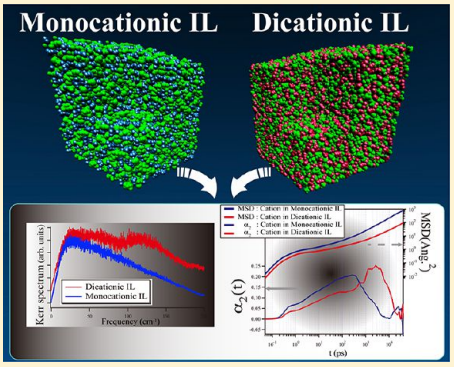

1. INTRODUCTION

The research fields of room temperature ionic liquids (ILs) have been developed rapidly, including the study of a new strategy to discover novel materials and the wide range of applications in diverse technological research areas.[1−9] It has been expected that ILs can be utilized as a replacement of organic solvents, reaction media, extraction liquids, lubrications, and so on.[1,2,7,8] Typical ILs consist of both cationic and anionic species, and the physical and chemical properties of these substances mostly depend on a combination of cations and anions in addition to their own properties. Therefore, we can expect to control and utilize the physical and chemical properties of ILs. Some research with molecular-level approaches has been reported.[3,4,10−21] For governing properties of ILs, it is essential for us to know the structural and dynamical features of ionic species in ILs. Also, it is desired to understand the characteristic of interionic interactions, since selection of suitable ionic species is required to prepare ILs for various kinds of specific purposes.

Recently, other than monocationic ILs, dicationic ILs have been the focus because of their unique features, including remarkable thermal stability, shear viscosities, surface tensions, and liquid densities larger than those of monocationic ILs, and a new class of dicationic ILs with various counteranions is expected to perform as interesting lubricants and solvents. From experimental points of view, several types of ammonium-based dicationic phosphate salt liquids were prepared and studied by Engel and co-workers.[22−26] Some of imidazolium-, pyridinium-, and ammonium-based dicationic ILs were synthesized by Ohno and co-workers.[27,28] Armstrong and co-workers identified physical properties such as thermal stability and shear viscosity for 39 dicationic ILs.[29] Also, Shirota et al. reported the physical properties, including liquid density, surface tension, and shear viscosity, of dicationic ILs, comparing them with those of monocationic ILs, as well as alkanediols and alkyl alcohols.[30] Theoretically, the electronic structure of dications and their complexes with counteranions was computed by an ab initio calculation.[31,32] The investigation of dicationic ILs with computer simulations was carried out.[33−35] Bodo et al. studied the structure of liquid phases for a series of germinal dicationic ILs with the $[NTf_2]^-$ anion with molecular dynamics (MD) simulation procedures and reported many common characteristics with corresponding monoimidazolic ILs.[34] In addition, they suggested that, also for dicationic ILs, low-k peaks reproduced from simulation results could be ascribed mainly to cation−

Received: November 8, 2012
Revised: December 27, 2012
Published: December 28, 2012

   dx.doi.org/10.1021/jp3110425 | J. Phys. Chem. B 2013, 117, 1136−1150

cation and anion−anion self-correlations, leaving the contribution of the interaction and segregation effects between alkyl chain groups in cations open to further discussion.

On the other hand, for dynamical properties on dicationic ILs, there have been very few studies. Recently, for ionic dynamics in dicationic ILs, we have investigated interionic interactions using femtosecond optical-heterodyne-detected Raman-induced Kerr effect spectroscopy (OHD-RIKES) to complement the structural information.[36] In the previous study,[36] we focused on the interionic dynamics and microscopic structure in a series of dicationic ILs and monoimidazolic counterparts with the $[NTf_2]^-$ anion in common and indicated that the exceptional difference on the low-frequency Kerr spectral profiles could emerge between 1-methyl-3-propylimidazolium bis(trifluoromethylsulfonyl)amide ($[C_3MIm][NTf_2]$) and 1,6-bis(3-methylimidazolium-1-yl)hexane bis(trifluoromethylsulfonyl)amide ($[C_6(MIm)_2][NTf_2]_2$). Then, we suggested for a possible interpretation of the origin of this exceptional difference that dicationic ILs imply the possibility to involve segregation structure and indicate imhomogeneity, depending on the alkyllene linker length of dicationic species. However, even though it was pointed out that these results in our previous paper[36] might include much important information related to dynamical properties in ILs, more details on the relation between structural and dynamical heterogeneities, including ionic motions, still have been left unresolved. In particular, on the connection between structural and dynamical heterogeneities, it has been pointed out that it is a difficult problem to deduce whole dynamical heterogeneity directly from the consideration of structural properties.[37] In addition, it should be noticed that while it is possible to observe structural information such as a structure factor experimentally, the analyses of dynamics spatially at a representative peak in the structure factor seem not to be feasible due to much slower relaxation in ILs than in usual liquid solvents. Thus, MD simulation is considered to be one of the appropriate and promising methods for tackling these subjects. Recently, toward access to molecular-level information, the interionic interaction and dynamics in ILs have been investigated through a complementary approach of both theoretical and experimental procedures.[13,14,38−43]

Related to the expected segregation structure in a series of dicationic ILs, this subject reminds us that experimental studies aimed at detecting the emergence of microscopic segregation or structural heterogeneity in ILs with long or intermediate alkyl chain group via X-ray and neutron scattering techniques have been reported extensively. Triolo et al. reported from the results obtained by small-angle X-ray scattering (SAXS) that a distinctive peak at the low-k (note that k denotes wavenumber below) region of less than 0.5 $Å^{-1}$, ascribed to the structural heterogeneity of ILs, for 1-alkyl-3-methylimidazolium ILs, $[C_nMIm][X]$ (X = Cl,[44] PF_6,[44] BF_4[45]), can be observed. On the distinctive low-k peak, Quitevis and co-workers[46] discussed microsegregation structures for a series of 1-alkyl-3-methylimidazolium ILs with bis(trifluoromethylsulfonyl)amide ($[NTf_2]^-$) anion, on the basis of the comparison of their X-ray scattering data with low-frequency Kerr spectra. Also, for $[C_nMIm][NTf_2]$ (n = 2, 4, 6, 8, 10, and 12), Umebayashi and co-workers[47] carried out a detailed analysis of the structural origin of low-k peaks in the range of 0.2−0.4 $Å^{-1}$ and studied the relation between the appearance of the low-k peaks and correlations among ionic species. From their analyses of X-ray diffraction and neutron scattering experiments including MD simulations, it was pointed out that liquid structures in the two real space regions of 5−8 and 8−15 Å contribute to the occurrence of the low-k peaks in $[C_nMIm][NTf_2]$ ILs and that correlations between imidazolium rings, imidazolium ring and $[NTf_2]^-$, or $[NTf_2]^-$ and $[NTf_2]^-$ could be attributed to the appearance of the low-k peaks. Also, they reported that the observed X-ray structure factor for $n > 6$ indicated characteristic low-k peaks, implying the structural heterogeneity of their ILs. In particular, from the experimental results with a small-angle neutron scattering technique, they examined for the case of $n \leq 10$ that the low-k peaks are not likely to be ascribed to correlations among the alkyl groups. In addition, they suggested that exclusive effects by the nonpolar alkyl chain aggregates are crucial to modify the characteristic length scale of cation−cation and anion−anion correlations.

Theoretically, the subjects mentioned above have been examined by simulation studies. Balasubramanian and co-workers performed MD simulations for $[BMIm][PF_6]$ and suggested that spatial correlations between the anions contribute to a characteristic peak in a low-k region.[48,49] For $[C_nMIm][PF_6]$ and $[C_nMIm][Cl]$, Margulis and co-workers concluded on the basis of MD simulations that the appearance of low-k peaks could be attributed to the distance between imidazolium ring and anion, which depends on the chain length of the long alkyl groups.[50] Also, recently, Castner, Margulis, and co-workers elucidated from the joint works of experiments and simulations that a low-k peak could be ascribed to cation−cation and anion−anion correlations.[51] Therefore, the investigation of the interionic correlations at a molecular level is promising to obtain a clear picture to interpret experimental results on the subject of structural features in ILs. Also, the investigation is expected to analyze how the degree Coulomb interactions are balanced with van der Waals interactions. Here, it should be noticed that each IL used in previous research mentioned above consists of monocation and monoanion, and thus, it is desirable to address these effects in the ILs containing polyvalent ionic species, since the strength of Coulomb interactions depends on the magnitude of the charge that each ion possesses.

In the light of the issues listed above, it is desirable to clarify how information on dynamical properties can be connected to the interpretation of structural properties. In this paper, we select $[C_3MIm][NTf_2]$ and $[C_6(MIm)_2][NTf_2]_2$ (hereafter denoted as monocationic IL and dicationic IL, respectively) for a comparative study (see Figure 1 for all the molecular structures of $[C_3MIm]^+$, $[C_6(MIm)_2]^{2+}$, and $[NTf_2]^-$, denoted as monocation, dication, and anion, respectively, below) and investigate ionic motions and dynamics in these ILs with the MD simulations. First, we carry out the analysis of interionic dynamics considering translational and librational motions to compare with the previous experimental results.[36] Second, on the basis of the computational results of structure factor, non-Gaussian parameters, that is, the deviation from Gaussian behavior, and intermediate scattering functions, we investigate structural effects arising from aggregations of ionic species on interionic interactions, and last, we show that the relation between spatial interionic correlations and dynamical heterogeneity in IL depends on the magnitude of the charge that each ion possesses, and the importance of discussing this relation is emphasized.

2. COMPUTATIONAL DETAILS

We carried out MD simulations with the DL_POLY molecular dynamics suite.[52] In all the simulations, we utilized the force field

dx.doi.org/10.1021/jp3110425 | J. Phys. Chem. B 2013, 117, 1136−1150

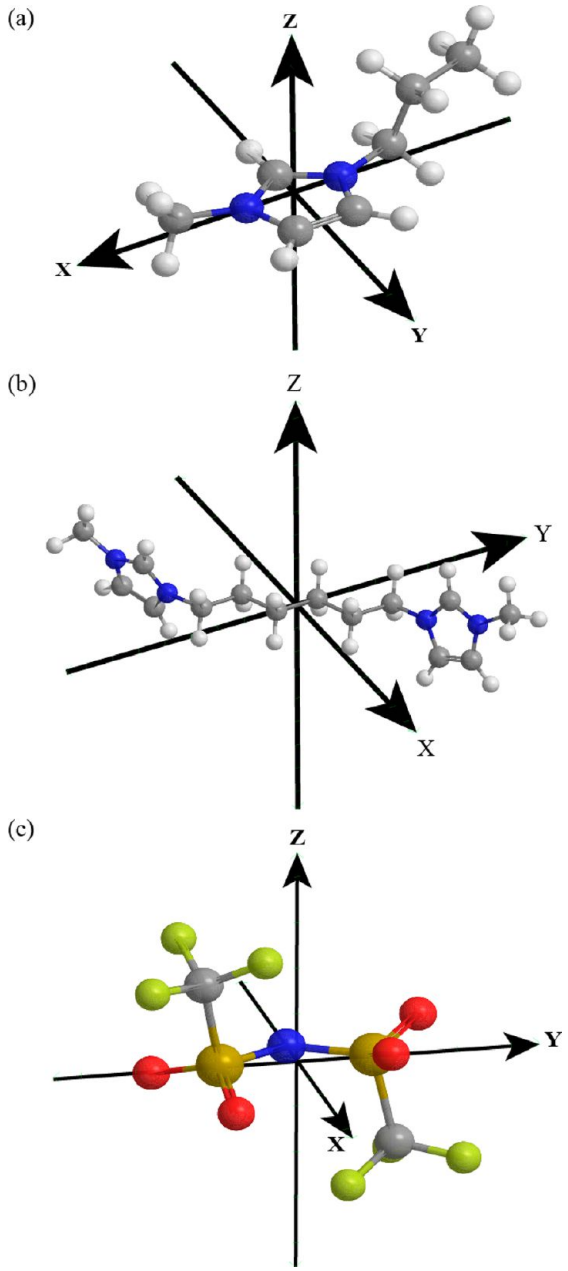

Figure 1. Structures and definitions of body-fixed coordinate axes for the cations and anion of the ILs used in this study: (a) $[C_3MIm]^+$, (b) $[C_6(MIm)_2]^{2+}$, and (c) $[NTf_2]^-$. In $[C_3MIm]^+$, the *X* direction is along the line connecting two nitrogen (blue colored) atoms in the ring, and the *Z* direction is set perpendicular to the ring plane and the *Y* direction axis. The *Y* direction is set in the ring plane orthogonal to both the *X* and *Z* axes. In $[C_6(MIm)_2]^{2+}$, the *Y* direction is along the line connecting two central carbon atoms in the carbon chain. The *Z* direction is set perpendicular to the *X* direction axis, and the plane consisted of the two central carbon atoms and one carbon atom preceding them in the carbon chain (that is, C−C−C plane), passing through the center of the bond between the two central carbon atoms. The *Y* direction is set in the plane orthogonal to both the *X* and *Z* axes. In $[NTf_2]^-$, the *Y* direction is along the line connecting two sulfur (dark yellow colored) atoms, and the *Z* direction is set perpendicular to the S−N−S plane and the *X* direction axis. The *X* direction is set in the S−N−S plane orthogonal to both the *Y* and *Z* axes.

parameters[53−55] for the monocation, the dication, and the anion, and since we focused mainly not on intramolecular but on interionic vibrations in this study, all the stretching bonds were constrained using the SHAKE algorithm.[56] In each IL system examined, 125 ion pairs (9000 atoms for the dicationic IL and 4625 for the monocationic IL, respectively) were set in a cubic box, and the periodic boundary condition was applied. Cutoffs for the real space part of the Coulombic and the Lennard-Jones interactions were set to 12 Å. The time step was 2 fs. The Ewald's summation technique was applied to the long-range Coulomb term.[57] At first, all the systems were equilibrated at 600 K for 5 ns in the *NVE* run and then gradually cooled down to 298 K with velocity scaling. Then, each system was equilibrated under *NPT* conditions for 3 ns with the Nosé−Hoover thermostats and barostats under 298 K and 1 atm. About 14 ns *NPT* simulations followed for computing densities for each system. The time constants of temperature and pressure were set to be 0.1 and 0.5 ps, respectively. We obtained the simulated density results of 1.494 g/mL for the monocationic IL and 1.521 g/mL for the dicationic IL. Our simulation results are in good accord with the observed data (1.476 and 1.546 g/mL for the monocationic and dicationic ILs, respectively).[30] On the basis of these results, the length of cubic box size was set to be 38.32 and 47.97 Å for the monocationic and dicationic ILs, respectively. Thereafter, we carried out *NVT* simulations at 298 K for a 25 ns equilibration run followed by a 40 ns production run. Simulation data were collected at every 50 fs during production runs.

For the calculation of the polarizability time correlation function, we computed gas-phase molecular polarizability tensors of the monocation, the dication, and the anion, respectively, using the Gaussian 03 program package.[58] We employed the DFT/B3LYP[59,60] level with the cc-pVDZ[61,62] basis sets. Table 1 displays the calculated molecular polarizability tensor elements. (See the Appendix for more computational details.)

3. RESULTS AND DISCUSSION

3.1. Vibrational Density of States (VDOS). The vibrational density of states (VDOS) can be calculated by the Fourier transformation of the autocorrelation function (ACF) of velocity, $\langle v_i(0)\, v_i(t)\rangle$, where $v_i(t)$ is the velocity of *i*th ionic species. The computed VDOS, as one of the dynamical aspects in the frequency domain, is shown in Figure 2. As pointed out previously,[14] modes corresponding to translational and rotational (librational) motions influenced by interionic interactions appear at lower frequencies (<100 cm^{-1}) in the VDOS profiles. Figure 2 exhibits the VDOS for the cations and anions in both the dicationic and monocationic ILs. For the cations, compared with the VDOS of the monocation, the VDOS of the dication indicates a broad profile spanning from 10 to 100 cm^{-1}. This broad peak is apparently indicative of a more heterogeneous dynamic environment in the dicationic IL. For this point, more detailed discussions and additional evidence with non-Gaussian parameters will be given later. In contrast, the VDOS of the anion for both the ILs exhibits a sharper peak around 20 cm^{-1}, which is characteristic of a low-frequency mode due to "rattling" motions in a cage comprised of counterions.[14,63]

3.2. Kerr Spectra and Ionic Dynamics. Though VDOS profiles can be useful for examining experimental Kerr spectra,[13,14,39,40] it is not feasible for us to compare computed VDOS profiles directly with observed Kerr spectra, since typical Kerr spectra come from the relaxation process of polarizability anisotropy, which also includes dynamical behavior other than translational dynamics. Therefore, we consider the ACF of total polarizability anisotropy of the system as a correlator for the

dx.doi.org/10.1021/jp3110425 | J. Phys. Chem. B 2013, 117, 1136−1150

Table 1. Components of the Molecular Polarizability Tensor Elements for $[C_3MIm]^+$, $[C_6(MIm)_2]^{2+}$, and $[NTf_2]^-$ (units in Å^3)

	$\alpha_{XX}{}^a$	$\alpha_{XY}{}^a$	$\alpha_{YY}{}^a$	$\alpha_{XZ}{}^a$	$\alpha_{YZ}{}^a$	$\alpha_{ZZ}{}^a$
$[C_3MIm]^+$	16.775	0.62064	12.248	−0.88954	0.24048	8.7994
$[C_6(MIm)_2]^{2+}$	29.493	8.9727	23.876	−0.051572	−0.071784	23.048
$[NTf_2]^-$	9.8855	1.4440×10^{-3}	13.577	-5.8531×10^{-4}	−1.0539	10.315

[a] *X*, *Y*, and *Z* directions are set as shown in Figure 1.

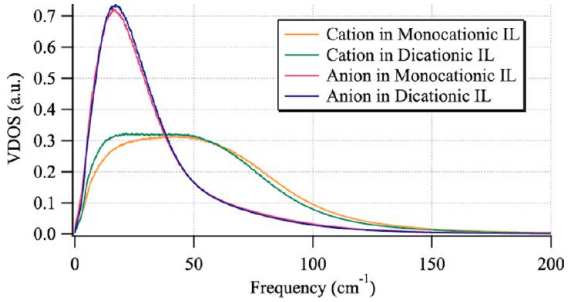

Figure 2. Comparison of computed VDOS of cations and anions of both monocationic and dicationic ILs ($[C_3MIm][NTf_2]$ and $[C_6(MIm)_2][NTf_2]_2$).

description of the dynamical behavior of ILs. From the Fourier transform of the time derivative of the ACF of the off-diagonal elements (anisotropy component) of the total polarizability of the system, we can compute Kerr profiles corresponding to the experimentally observed Kerr spectra. Also, the total polarizability of the system can be decomposed into cation, anion, and cation−anion cross-correlation components with MD simulation data.[14,41] For theoretical and computational details, readers should refer to references previously reported[14,41] and the Appendix. Both the experimental results[36] and computed Kerr spectra are displayed in Figure 3a,b. As seen in the figures, calculation results are qualitatively in good accord with the observed spectra for both the dicationic and monocationic ILs, though we can see a discrepancy between 100 and 150 cm^{-1}. The improvement of the profiles is left to further refinements of force field parameters. Therefore, we concentrate on the spectral profile below 100 cm^{-1} and its origin.

In Figure 4a, the computation results for the decomposition analysis of the Kerr spectrum of the monocationic IL are shown. It is seen that the cation−anion cross-correlation mainly contributes to the total Kerr spectrum at the frequency region up to 100 cm^{-1}, while both the cation and the cross-correlation components participate in the total profile almost equivalently at a higher frequency region than 100 cm^{-1}. In contrast, the contribution of the anion component is less than others at the whole frequency region. The calculation results of the dicationic IL given in Figure 4b also indicate a similar profile to the case of the monocationic IL, except that a characteristic peak appears between 50 and 100 cm^{-1}. These observations indicate the following two aspects. The first is that the cation−anion cross-correlation dominantly contributes to the Kerr spectrum profile for each IL. The second aspect is that a different contribution to the Kerr spectra between the cations and the anions implies that the structural deviation from a symmetric form is larger in the monocation and the dication than in the anion. The latter is consistent with the fact that the experimentally observed Kerr transients of ILs mainly consist of signals coming from asymmetric ionic species.[13] The origin of the characteristic peak at between 50 and 100 cm^{-1} in the dicationic IL will be discussed later.

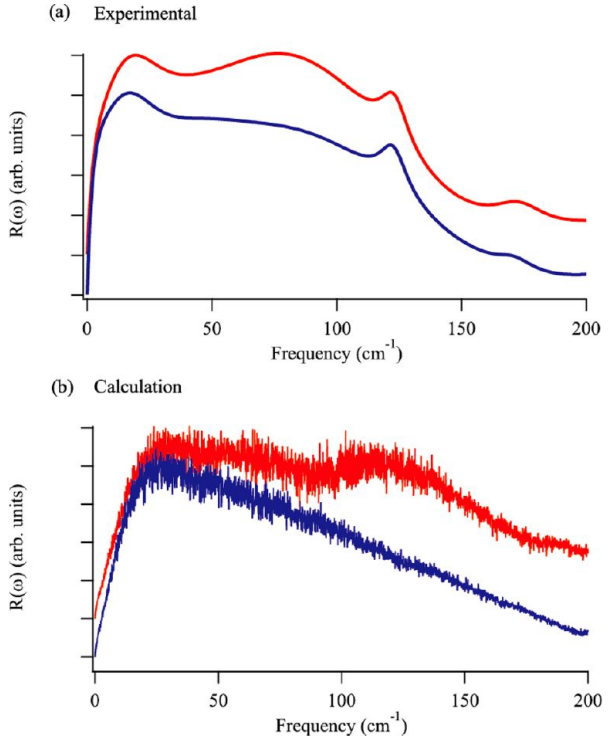

Figure 3. Comparison of the calculated Kerr spectra for monocationic and dicationic ILs ($[C_3MIm][NTf_2]$, blue; $[C_6(MIm)_2][NTf_2]_2$, red) with the experimental Kerr spectra:[36] (a) the experimental Kerr spectra and (b) the calculated Kerr spectra. Note that the spectra for the dicationic IL are shown with an offset.

To study the dynamics in ILs further, it is possible to evaluate an interaction-induced effect due to reorientational motions, employing the projection scheme for the separation of reorientational component from collision-induced component.[14,41,64,65] Theoretical and computational details are given briefly in the Appendix. Figure 5a,b displays the decomposition results of the Kerr spectra as the reorientational, collision-induced, and reorientational collision-induced cross-correlation parts for the monocationic and dicationic ILs, respectively. It is found that the reorientational motions of cations and anions contribute dominantly, while the collision-induced and reorientation−collision cross-correlation components do not. This indicates that the reorientational motion of ions mainly participates in the Kerr spectrum profile. Only from these results, however, it is difficult to discuss how a characteristic reorientational (rotational) motion, such as librational motion, contributes to the Kerr spectrum profile. Therefore, we study the librational dynamics further below.

3.3. Librational Dynamics. The decomposition analysis of the Kerr spectra exhibits that modes corresponding to reorientational (rotational) or librational motion have characteristic Raman intensities. The ACF of the total angular momentum of cation and anion molecules and its power spectrum enable us to carry out an analysis of librational modes in detail. To separate

dx.doi.org/10.1021/jp3110425 | J. Phys. Chem. B 2013, 117, 1136−1150

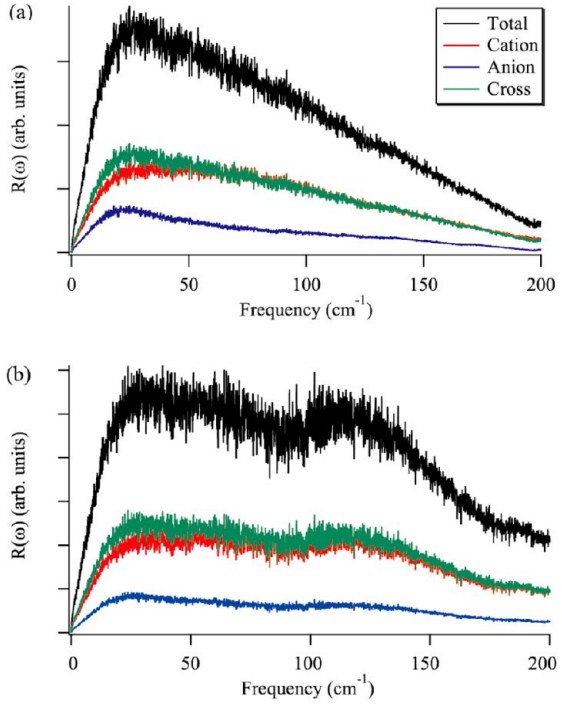

Figure 4. Decomposition of the computed Kerr spectra into the cation and anion contributions and the cation−anion cross-correlation component: (a) monocationic IL ($[C_3MIm][NTf_2]$) and (b) dicationic IL ($[C_6(MIm)_2][NTf_2]_2$).

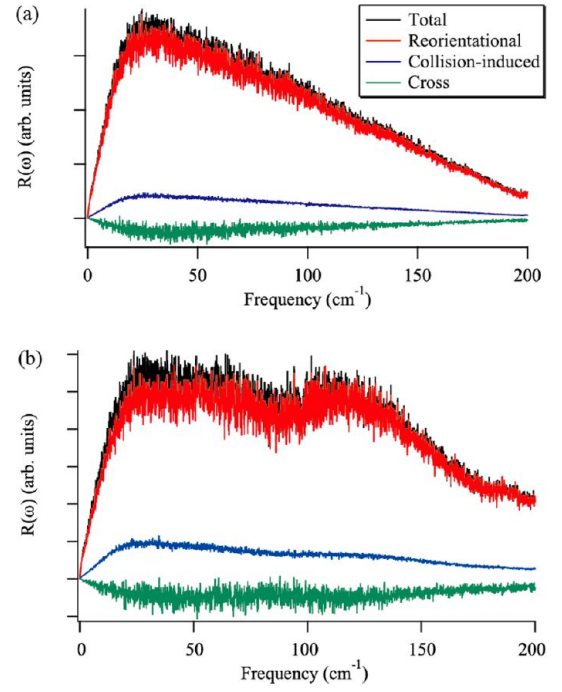

Figure 5. Decomposition of the computed Kerr spectra into the reorientational and collision-induced components and the cross-term contribution: (a) monocationic IL ($[C_3MIm][NTf_2]$) and (b) dicationic IL ($[C_6(MIm)_2][NTf_2]_2$).

the librational modes, we set the body-fixed coordinate axes, *X*, *Y*, and *Z*, in the monocation, the dication, and the anion, respectively (see Figure 1). Then, the component of librational motion about the body-fixed coordinate axes set in each system can be obtained from the projection of the total angular momentum vector, **J**, onto each axis, $J_i = \mathbf{J}\cdot\mathbf{I}_i$ (i = *X*, *Y*, and *Z*), where $\mathbf{I}_i$ represents the unit vector. The momentum ACF (MACF) of each component, $C_i(t) = \langle J_i(t)\cdot J_i(0)\rangle$ (i = *X*, *Y*, and *Z*), was computed. Results are displayed in Figures 6a,c and 7a,c.

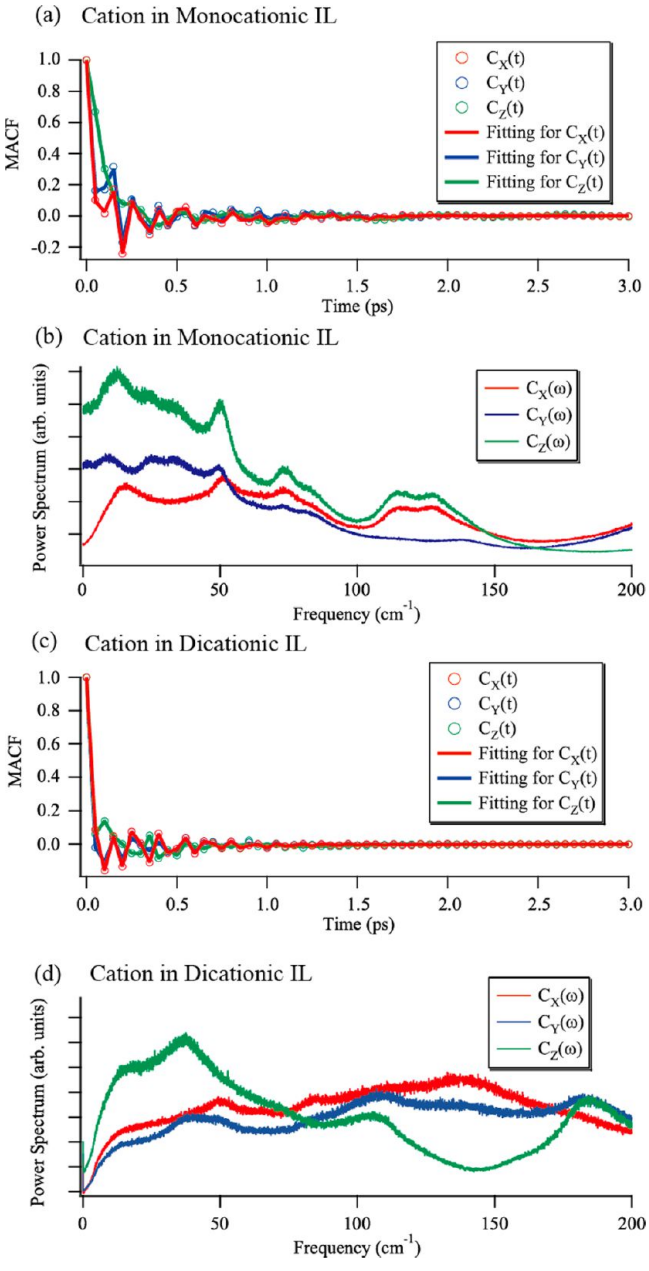

Figure 6. (a) Momentum autocorrelation functions (MACFs) of monocation ($[C_3MIm]^+$). (b) Power spectra of the MACFs. (c) MACFs of dication ($[C_6(MIm)_2]^{2+}$). (d) Power spectra of the MACFs. (See text and Figure 1 for C_X, C_Y, and C_Z.)

It is found that an autocorrelator for each rotational motion shows remarkable damped oscillations different from the behavior of free rotating molecules. These observations indicate that the contribution of the sterically hindered rotational motion to a decaying of the MACFs is larger than in less-hindered motion. Therefore, this contribution has an effect on the low-frequency region of the power spectrum.

To fit computed MACF curves of the monocation and the dication, we employed the model of Gaussian-distributed oscillators with the functional form[66−68]

dx.doi.org/10.1021/jp3110425 | J. Phys. Chem. B 2013, 117, 1136−1150

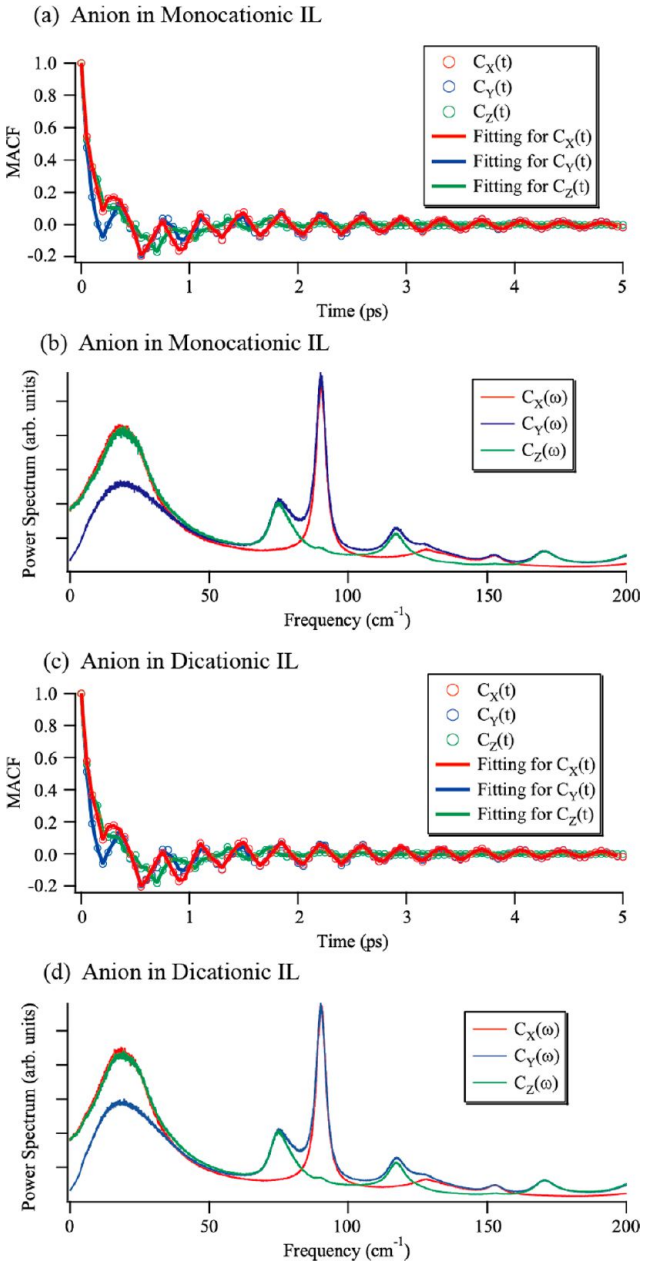

Figure 7. (a) Momentum autocorrelation functions (MACFs) of $[NTf_2]^-$ in monocationic IL ($[C_3MIm][NTf_2]$). (b) Power spectra of the MACFs. (c) MACFs of $[NTf_2]^-$ in dicationic IL ($[C_6(MIm)_2][NTf_2]_2$). (d) Power spectra of the MACFs. (See text and Figure 1 for C_X, C_Y, and C_Z.)

$$C(t) = \sum_{i=1}^{n} a_i \cos(2\pi\omega_i t) \exp\left[-\frac{(c\Delta_i t)^2}{2}\right] \quad (1)$$

where ω_i and Δ_i represent the frequency and inhomogeneous width of the ith mode, respectively, and c means the speed of light. A reasonable fit was obtained with $n = 8$, except for $C_Z(t)$ of the dicationic IL ($n = 9$). Table 2 shows a series of representative fitted parameters for $a_i > 0.1$ (10%) and $\omega_i < 200$ cm^{-1} for cations. (See the Supporting Information for all the fitted parameters.) The power spectra of the $C_X(t)$, $C_Y(t)$, and $C_Z(t)$ are displayed in comparison in Figure 6b,d. Here, it should be noticed that the model functional form used here explicitly includes damping effects influenced by the inhomogeneous behavior.

For the monocation, according to the results of a_i and a_2 in Table 2, about 30−40% of cation motions have librational modes lower than 100 cm^{-1} about the X and Y axes and about 60% about the Z axis. In the power spectra, it is found that three main librational modes consist of frequency regions, centered at around 25, 75, and 120 cm^{-1} for all the correlators. Also, broad spectral features, extending from 0 to 150 cm^{-1}, result from the large value of Δ_n for each frequency. On the other hand, for the dication, about 40% of cation motions show librational modes only about the Z axis, and each frequency is lower than 100 cm^{-1}. $C_X(\omega)$ and $C_Y(\omega)$ indicate similar behavior with two common librational mode regions at between 100 and 200 cm^{-1}. In contrast, librational motion about the Z axis possesses a low-frequency mode at around 35 cm^{-1}. Also, at around 180 cm^{-1}, distinctive modes about the Y and Z axes with large contribution were obtained, while the spectral feature of the $C_X(\omega)$ becomes broad there since the value of Δ_2 is much larger than the others.

In particular, it has been pointed out experimentally[69] that broad spectra profiles in imidazolium cation based ILs due to the contribution of cation species are often observed at around 80 cm^{-1} and that the contribution from anion species is at around 20 cm^{-1}. Here, first we discuss the difference of the Kerr spectra between the monocationic and dicationic ILs on the basis of the analysis of the librational modes of the monocation and the dication. Table 2 includes frequencies, about 120 cm^{-1} (ω_3 for the X and Z axes for the monocation and ω_1 for the X and Y axes for the dication, respectively), corresponding to representative peaks in the experimentally observed Kerr spectral profiles (see Figure 3a). Interestingly, it is found that a distinctive frequency at 98 cm^{-1} (ω_2 for the Z axis) appears for the dication. This frequency is consistent with the characteristic peak seen in the Kerr spectrum of the dicationic IL at between 50 and 100 cm^{-1}, while it is not observed in the monocationic IL. From our analyzes mentioned above, this characteristic peak originated

Table 2. Fit Parameters of the Angular Momentum Autocorrelation Functions $C_X(t)$, $C_Y(t)$, and $C_Z(t)$ for $[C_3MIm]^+$ and $[C_6(MIm)_2]^{2+}$ [a] in each IL

	a_1	ω_1	Δ_1	a_2	ω_2	Δ_2	a_3	ω_3	Δ_3
					$[C_3MIm]^+$				
X	0.13012	33.150	88.645	0.14392	72.416	88.217	0.15791	121.89	124.06
Y	0.27041	28.932	113.00	0.14864	74.462	121.89	–	–	–
Z	0.53865	27.979	149.11	0.10789	77.090	70.694	0.1733	120.70	112.84
					$[C_6(MIm)_2]^{2+}$				
X	0.15432	128.05	191.74	0.49548	183.14	489.50	–	–	–
Y	0.40922	113.24	288.79	0.15394	192.43	155.98	–	–	–
Z	0.16170	35.288	83.415	0.22999	98.399	194.57	0.15031	184.63	121.94

[a] ω_n and Δ_n (n = 1, 2, and 3) are in cm^{-1}.

dx.doi.org/10.1021/jp3110425 | J. Phys. Chem. B 2013, 117, 1136−1150

Table 3. Fit Parameters of the Angular Momentum Autocorrelation Functions $C_X(t)$, $C_Y(t)$, and $C_Z(t)$ for $[NTf_2]^-$ in Monocationic and Dicationic ILs ($[C_3MIm][NTf_2]$ and $[C_6(MIm)_2][NTf_2]_2$)[a]

	a_1	ω_1	Δ_1	a_2	ω_2	Δ_2	a_3	ω_3	Δ_3	$b/10^{-4}$	ν	Γ
						$[NTf_2]^-$ in the Monocationic IL						
X	0.24266	18.541	56.553	0.31181	30.417	176.79	–	–	–	7.0000	91.967	1.5023
Y	0.17344	27.789	73.433	0.34629	86.542	274.86	–	–	–	7.0000	91.967	1.5023
Z	0.16629	18.535	51.073	0.26533	21.876	109.16	0.22200	70.189	217.20	–	–	–
						$[NTf_2]^-$ in the Dicationic IL						
X	0.29768	18.220	59.753	0.2685	33.815	154.32	–	–	–	7.0000	91.967	1.5023
Y	0.10587	14.571	42.298	0.19006	27.767	71.997	0.33293	86.006	266.43	7.0000	91.967	1.5023
Z	0.19016	18.187	53.548	0.27040	23.027	104.78	0.21241	71.003	205.62	–	–	–

[a] ω_n and Δ_n (n = 1, 2, and 3), ν, and Γ are in cm^{-1}.

from the librational motion of the dication about the Z axis with relatively larger moment compared with about other axes. In addition, as shown in Table 2, the number of frequency modes lower than 100 cm^{-1} for the monocation is greater than that for the dication, and the widths of modes (the values of Δ) corresponding to the frequency modes lower than 100 cm^{-1}, in particular, for the Z axis, are larger for the dicationic IL than for the monocationic IL. Considering that lower librational mode corresponds to weaker restoring force, this indicates that there are more monocations weakly bound to surrounding ions compared with the dication. Therefore, it is likely that the effect of inhomogeneous environment on the Kerr spectra appears in the dicationic IL more remarkably than in the monocationic IL.

In contrast to the cations, the results of the anion show remarkably different aspects. In particular, while a reasonable fit is obtained with eq 1 (n = 9) for $C_Z(t)$, the following modified functional form of eq 1 is required for a best fitting of the $C_X(t)$ and $C_Y(t)$

$$C(t) = \sum_{i=1}^{n} a_i \cos(2\pi\omega_i t) \exp\left[-\frac{(c\Delta_i t)^2}{2}\right] + b \sin(2\pi\nu t) \exp(-c\Gamma t) \quad (2)$$

where the auxiliary term corresponds to the so-called resonance-type behavior corresponding to the forced oscillation,[70,71] and ν and Γ represent the frequency and its peak width, respectively. The MACFs and its power spectra are displayed in Figure 7. Also, the results of representative fitted parameters for $a_i > 0.1$ (10%) and $\omega_i < 200$ cm^{-1} are shown in Table 3. (See the Supporting Information for all the fitted parameters.) From the results of coefficients a_i in Table 3, in both the monocationic and dicationic ILs, about 50−60% of anion motions have librational modes lower than 100 cm^{-1} about the X and Y axes and about 70% about the Z axis. Also, each librational mode higher than 100 cm^{-1} has a small contribution of less than 10%. In the power spectra, the large values of Δ_2 and Δ_3 reflect broadening width in spectral features (>50 cm^{-1}) in both the ILs. Both the $C_Y(\omega)$ and $C_Z(\omega)$ include peaks at around 70 cm^{-1}, while the $C_X(\omega)$ does not. It is considered that these differences depend on to what degree a librational mode, about each axis, is modulated due to interactions with environment. Thus, compared with the librational motion about the X axis, the librational motion about the Y and Z axes is likely to be influenced by stronger interactions with the surrounding cations and anions, which might cause so-called cages in each IL. Here, it should be noted that the homogeneous feature of ionic motions effective to the origin of the spectral broadening could be caused in both the dicationic and monocationic ILs as well as the inhomogeneous behavior discussed above.

For resonance-type sharp peaks, the same fitted parameters are obtained in both the monocationic and dicationic ILs. As seen in Figure 7b,d, the power spectra for the anion in both the ILs are very similar to each other. It is found that the sharp peak at around 90 cm^{-1} appears in both the ILs. In fact, a strong intramolecular vibrational band at about 120 cm^{-1} has been observed in the Kerr spectra of not only aromatic and nonaromatic cation based ILs with $[NTf_2]^-$ but also solutions including lithium bis(trifluoromethylsulfonyl)amide.[72] This sharp peak frequency is consistent with the reported quantum chemical calculation results[36] of the anion which showed the frequency modes with relatively large Raman activity of 105.31 cm^{-1} with B3LYP/aug-cc-pVDZ[59−62,73] level of theory and 105 cm^{-1} with B3LYP/6-31+G(d, p),[69] respectively. Therefore, this sharp peak is considered to be an intermolecular motion coupled to the vibrational mode intrinsic to the anion.

On the role of the anion in each IL, we can see the contribution of the anion to the total Kerr profiles at frequencies lower than 50 cm^{-1}. The power spectra in Figure 7b,d indicate that peak intensities at frequencies lower than 50 cm^{-1} are much larger than at the following frequencies, except for the sharp peaks. Therefore, the dominant contribution of the anion to the total Kerr profiles is due to low-frequency modes (<50 cm^{-1}) coming from librational motion of the anion, as previously pointed out.[69] Also, the contribution of the cations due to reorientational or librational motion to the Kerr spectra is influenced by interionic interactions. These are consistent with the results that the cation−anion cross-correlation contributes as equal as the cation component in both the monocationic and dicationic ILs, as shown in Figure 4.

3.4. Dynamics and Spatial Correlation in ILs. Dynamics of ILs are largely related to spatial correlation. First, we examine heterogeneous dynamical behavior of cations and anions in the ILs, and then, the relaxation of density correlations at a specified length scale will be discussed using computed intermediate scattering functions in this section.

3.4.1. Dynamical Behavior (Diffusive Motion and Non-Gaussian Parameter). Figure 8a,b displays the results calculated for the mean-squared displacement (MSD) of the center of mass of ions, $\langle \sum_{i=1}^{N} [\mathbf{r}_i(t) - \mathbf{r}_i(0)]^2 \rangle$, where $\mathbf{r}_i$ is the position vector of the center of mass of the ion i, and, in comparison, the so-called second-order non-Gaussian parameter,[74−76]

$$\alpha_2(t) = \frac{3\langle r^4(t) \rangle}{5\langle r^2(t) \rangle^2} - 1 \quad (3)$$

where $r(t)$ is the displacement of an ion at time t with respect to its position at t = 0. In Figure 8a,b, the MSDs of the monocation, the dication, and the anion in both the monocationic and

dx.doi.org/10.1021/jp3110425 | J. Phys. Chem. B 2013, 117, 1136−1150

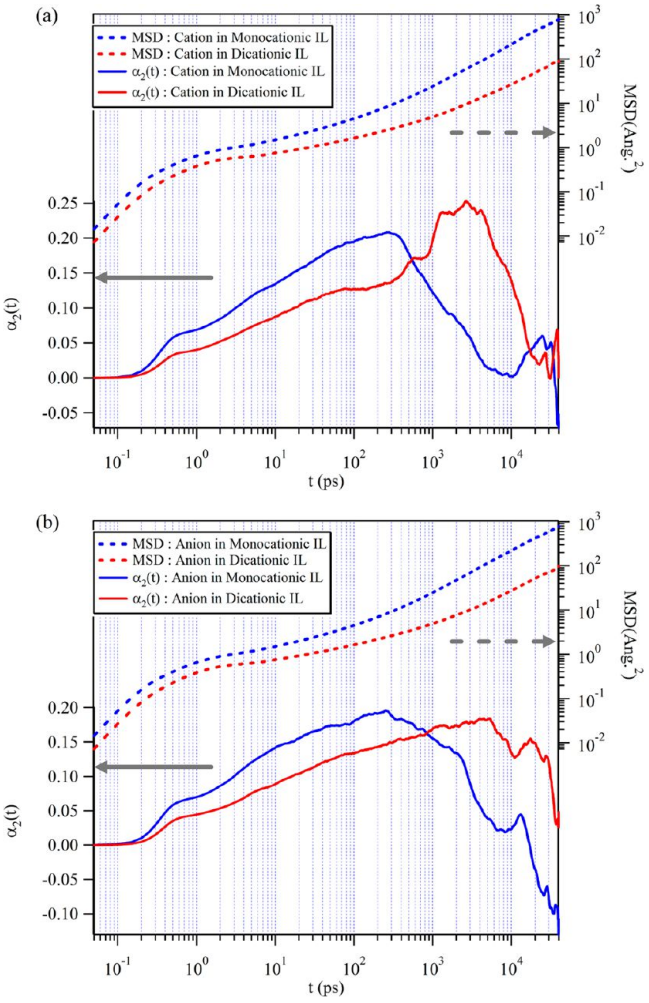

Figure 8. MSDs and non-Gaussian parameters for (a) the cation and anion of monocationic IL ($[C_3MIm][NTf_2]$) and (b) the cation and anion of dicationic IL ($[C_6(MIm)_2][NTf_2]_2$).

dicationic ILs indicate three typical dynamic ranges (regions), respectively. Also, in the Supporting Information (Figure S1), we show $\beta(t) = d[\log(MSD)]/d[\log(t)]$ for both the cations and the anions to examine a diffusive regime.[11] From Figure S1 (Supporting Information), these curves represent that only after 15 ns does $\beta(t)$ become close to 1, which indicates the diffusive regime.

For the monocation, the first region is a microscopic regime until about 10−20 ps. The second is a crossover regime until about 2 ns, and the third region is a sublinear time dependence toward 40 ns. Also, $\alpha_2(t)$ shows the features including a representative peak. The representative peak is located at about 300 ps. In addition, a remarkable deviation from Gaussian behavior starts from about 0.3 ps and it ends at the beginning of the crossover regime ($t \sim 20$ ps). It is found that the remarkable deviation behavior at the short-time regime corresponds to the microscopic region of the MSD, while the representative peak at the long-time regime (at about 300 ps) appears in the center of the crossover regime of the MSD. The behavior of the short- and long-time regimes of both MSD and $\alpha_2(t)$ depends on the ionic species considered. As seen in Figure 8a, for the typical three regions of the MSD of the dication, the microscopic regime as the first region is until about 10−20 ps. However, the crossover regime as the second is extended until about 10 ns, and third region is until 40 ns. It is seen in the profile of the $\alpha_2(t)$ of the dication that a gradual increase of deviation from Gaussian behavior is included toward the representative peak at around 3 ns through the intermediate region of the crossover regime ($t \sim 1$ ns). These results imply that the motion of the dication, which is massive, becomes slower than that of the monocation and that its slowness influences the relaxation behavior after the crossover regime. These observations are consistent with our results that the magnitude of the deviation from the Gaussian behavior is remarkably larger for the dication than for the monocation, as shown in Figure 8a.

On the other hand, for the anion in each IL, $\alpha_2(t)$ includes characteristic features similar to those of the cation. In particular, the representative peak at the long-time region is shifted to about 5 ns, while the deviation behavior at the short-time region is almost at the same time region as the cation. The time regimes where the representative peak appears are in qualitatively accord with those of the monocation and the dication, respectively, as seen in Figure 8b. Therefore, considering that the Kerr spectrum is modified depending on the relaxation behavior of the experimentally detected perturbed system, the difference of relaxation behavior (non-Gaussian behavior) between the monocation and the dication is reflected in the distinction of Kerr profiles between the monocationic and dicationic ILs, and this is also consistent with the discussion on the relation between the librational dynamics and the Kerr spectra mentioned above.

3.4.2. Spatial Correlation and Interionic Interactions. With the simulation results of radial distribution function (RDF) for atomic species of type i and j, $g_{ij}(r)$, the total X-ray structure factor, $S(k)$, can be computed using following equation:

$$S(k) = \frac{\sum_i \sum_j n_i n_j f_i(k) f_j(k)}{\{\sum_l (n_l f_l(k))\}^2} \int_0^r 4\pi r^2 \rho_0 (g_{ij}(r) - 1) \frac{\sin(kr)}{kr} dr + 1 \quad (4)$$

where n_i and $f_i(k)$ represent the number and the atomic scattering factor[77] of atom i, respectively. ρ_0 is the number density. In Figure 9, we display the calculated static structure factor, $S(k)$, for both the monocationic and dicationic ILs.[78]

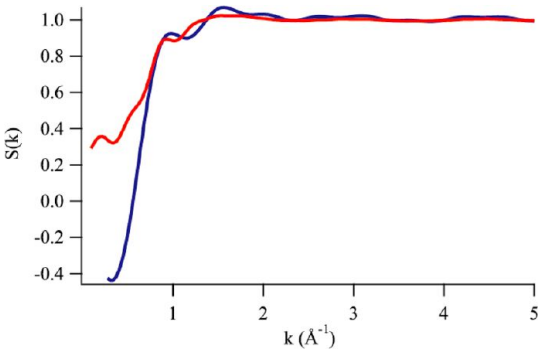

Figure 9. Computed total X-ray structure factors for monocationic and dicationic ILs ($[C_3MIm][NTf_2]$, blue; $[C_6(MIm)_2][NTf_2]_2$, red).

In the range of $k \leq 2$ Å^{-1}, which includes information about interionic interactions, $S(k)$ indicates two main peaks at around 0.90 and 1.50 Å^{-1} in both the systems. The former and latter peaks for the dicationic IL are slightly shifted to lower-k region in comparison with those for the monocationic IL. These are consistent with the observed results[46,47] that the profile of $S(k)$

dx.doi.org/10.1021/jp3110425 | J. Phys. Chem. B 2013, 117, 1136−1150

can be largely modulated depending on the alkyl chain length, which modifies interionic interactions including Coulombic and van der Waals interactions. The profile of $S(k)$ for the dicationic IL shows a small shoulder peak at around 0.5 Å^{-1}, while it does not appear for the monocationic IL. This result is also in agreement with the experimental results that a similar shoulder structure at around 0.5 Å^{-1} is intensified with increasing n (>4) in $S(k)$s of $[C_nMIm][NTf_2]$ ILs.[46] Also, a low-k peak is clearly seen at around 0.20 Å^{-1} for the dicationic IL. Similar low-k peaks have been experimentally observed and reported for other IL systems including monocations with a long alkyl chain,[50,51] but those do not emerge for the monocationic IL in the current study. Thus, remarkable differences in the $S(k)$ between the monocationic and dicationic ILs could be attributed to the change of interionic interactions due to the alteration of alkyl chain or linkage chain length and the difference of charge number between the monocation and the dication in cationic species. Also, in the Supporting Information (Figure S2), we show the computed partial structure factors for anion−anion, cation−anion, and cation−cation correlations for the dicationic IL. From Figure S2 (Supporting Information), it is likely that the low-k peak could be related to anion−anion and cation−anion correlations, mainly. On this point, more detailed analyses will be given later. Here, it should be noticed that, according to a previous report for $[C_nMIm][NTf_2]$,[47] a similar characteristic low-k peak appears for $n > 6$, but in our study, the dicationic IL containing six alkyl groups shows the low-k peak, indicating the heterogeneity of ILs.

3.4.3. Structural Relaxation in ILs. As mentioned in the preceding subsections, it is obviously found that the dynamics of an anion is spatially correlated with that of a countercation. At first, to investigate structural relaxation, we consider the self-part of the intermediate scattering function[79] defined as

$$F_s(k, t) = \frac{1}{N}\sum_{j=1}^{N} \langle \exp[i\mathbf{k}\cdot\{\mathbf{r}_j(t) - \mathbf{r}_j(0)\}]\rangle \quad (5)$$

where $k = |\mathbf{k}|$. Here, we select the k values corresponding to four representative peaks shown in Figure 9. The computed results for the cations and the anions in both the monocationic and dicationic ILs are displayed in Figures 10 and 11 for the monocationic IL (k = 0.23, 0.50, 0.90, and 1.50 Å^{-1}) and the dicationic IL (k = 0.20, 0.50, 0.90, and 1.50 Å^{-1}), respectively. As seen in Figures 10 and 11, $F_s(k,t)$ exhibits the two-step decay feature characteristic of supercooled liquids and glass formers.[80−82] This result is not surprising, since similar results have been reported for ILs.[48,63,83] Two dynamic regimes consist of a fast relaxation process at short time scales (β relaxation) and the following process at longer time scales, where ions escape the cage formed by their surrounding ions (α relaxation).

Also, considering that broad features are observed around the $\alpha_2(t)$ peak and characterized by the full width at half-maximum (fwhm)[76] (see Figure 8), we notice in the results of the dication (Figure 10) that, for low-k values (k = 0.20 and 0.50 Å^{-1}), the time region (∼10 ns) corresponding to the fwhm of the $\alpha_2(t)$ peak does not encompass the whole range of the α relaxation but covers it almost entirely as k becomes larger. In contrast, for the monocation, the time range (∼1 ns) covers almost completely all the values of k (see Figures 8a and 10). Similarly, we can see in the results of the anion in the dicationic IL that, at k = 0.20, 0.50, and 0.90 Å^{-1}, the time region (∼10 ns) to the fwhm of the $\alpha_2(t)$ peak does not cover the total range of the α relaxation, while this relaxation almost entirely finishes within the time region for the anion in the monocationic IL (∼1 ns) at all the values of k (see Figures 8b and 11). Therefore, it is found that the non-Gaussian behavior of ILs can influence the decay of the spatial density−density correlation, depending on the k value. In particular, the effect appears significantly in the dicationic IL compared to that in the monocationic IL. This indicates that the dynamical behavior of a germinal dicationic IL is clearly different from that of its monocationic imidazolium counterpart.

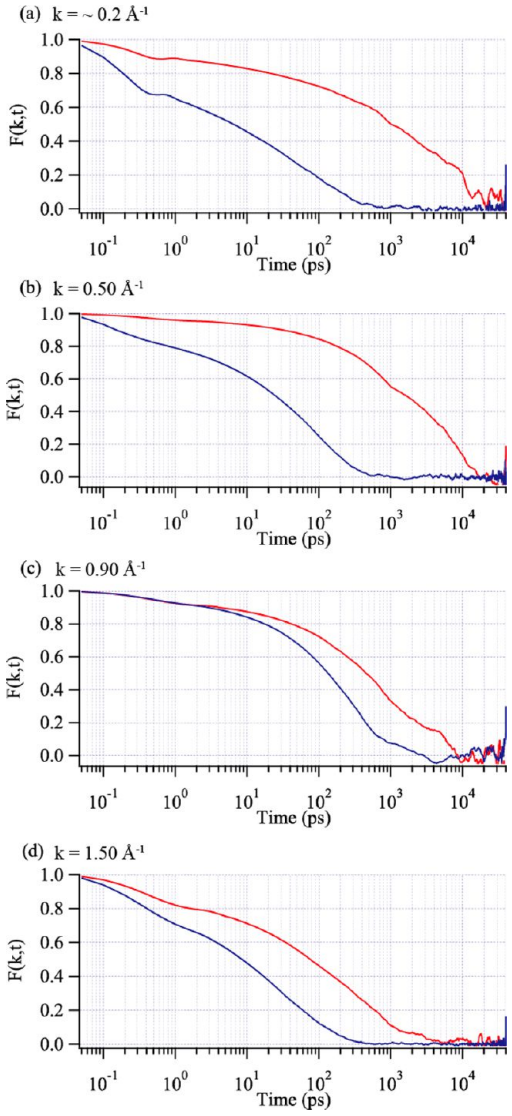

Figure 10. Self-intermediate (incoherent) scattering function, $F_s(k,t)$, of monocation ($[C_3MIm]^+$, blue) and dication ($[C_6(MIm)_2]^{2+}$, red) at (a) k = 0.23 Å^{-1} for the monocation and 0.20 Å^{-1} for the dication, (b) k = 0.50 Å^{-1}, (c) k = 0.90 Å^{-1}, and (d) k = 1.50 Å^{-1}.

Furthermore, in Figure 11a, we can observe, at the low-k regions (k = 0.20 and 0.23 Å^{-1}) corresponding to spatially long-range, the presence of a dip in the correlator at around 0.5 ps for both the monocationic and dicationic ILs, respectively. These results are similar to the relaxation behavior of a viscous melt of silica, as pointed out by Horbach and Kob.[84] According to their report, the appearance of the dip corresponds to the "rattling" motion of SiO_2 in the cage formed by their neighbors and its network.[84] Here, it should be noted that the ions that form the cage move themselves, too. Nevertheless, it is considered that the dip shown in the current results implies the rattling motion of the anion in the cage formed by surrounding cations. With the time duration of the dip we observed in Figure 11a (∼0.35 ps), we

dx.doi.org/10.1021/jp3110425 | J. Phys. Chem. B 2013, 117, 1136−1150

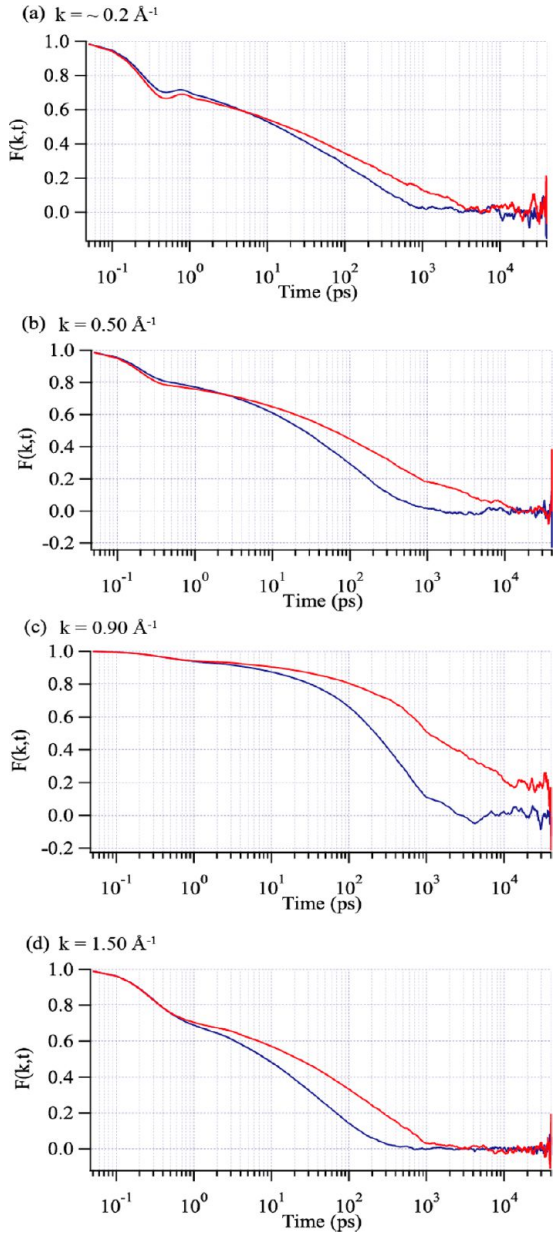

Figure 11. Self-intermediate (incoherent) scattering function, $F_s(k,t)$, of $[NTf_2]^-$ in monocationic (blue) and dicationic (red) ILs ($[C_3MIm][NTf_2]$ and $[C_6(MIm)_2][NTf_2]_2$) at (a) k = 0.23 Å^{-1} in the monocationic IL and 0.20 Å^{-1} in the dicationic IL, (b) k = 0.50 Å^{-1}, (c) k = 0.90 Å^{-1}, and (d) k = 1.50 Å^{-1}.

could roughly estimate the value of ~95 cm^{-1} for a frequency corresponding to this duration. The rattling motion is composed of the combination of the rotational motions or librations about the X and Y axes shown in Figure 1. Thereby, after the time regime when the anion leaves the cage completely, the structural relaxation of the system (α relaxation) follows.

3.4.4. Connection of Collective Dynamics of ILs to Spatial Correlations between Ions. Next, to study the relation between collective dynamics and spatial correlations of ionic species, we consider the coherent intermediate scattering function,[76,79] $F_{coh}(k,t)$, defined as

$$F_{coh}(k,t) = \frac{1}{N}\sum_{i=1}^{N}\sum_{j=1}^{N}\langle \exp[i\mathbf{k}\cdot\{\mathbf{r}_j(t) - \mathbf{r}_i(0)\}]\rangle \quad (6)$$

which describes the collective motion of cations and anions in the system. The computed results are displayed in Figure 12 for the

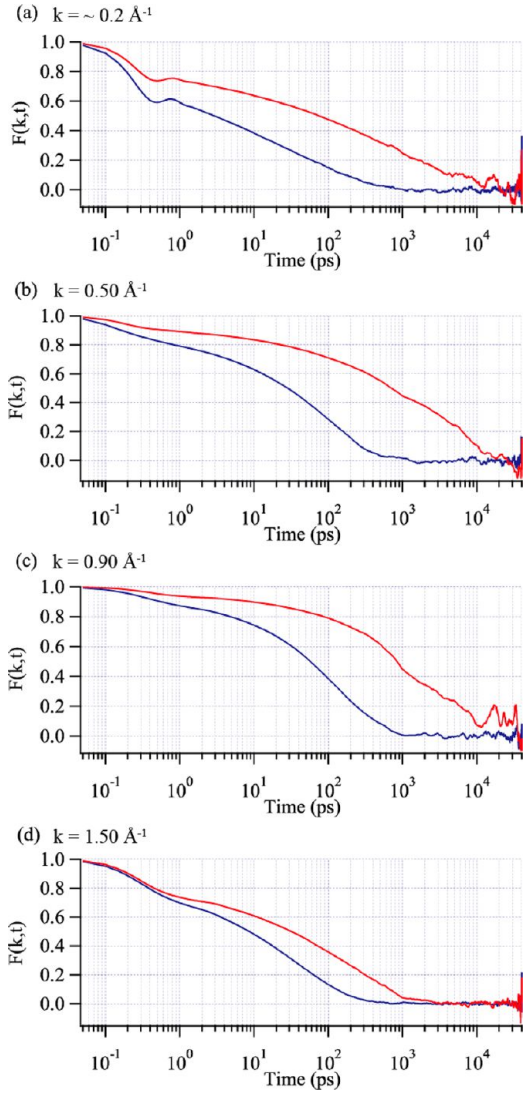

Figure 12. Coherent intermediate scattering function, $F_{coh}(k,t)$, of monocationic and dicationic ILs ($[C_3MIm][NTf_2]$, blue; $[C_6(MIm)_2][NTf_2]_2$, red) at (a) k = 0.23 Å^{-1} in the monocationic IL and 0.20 Å^{-1} in the dicationic IL, (b) k = 0.50 Å^{-1}, (c) k = 0.90 Å^{-1}, and (d) k = 1.50 Å^{-1}.

monocationic IL (k = 0.23, 0.50, 0.90, and 1.50 Å^{-1}) and the dicationic IL (k = 0.20, 0.50, 0.90, and 1.50 Å^{-1}), respectively. As shown in Figure 12, the coherent scattering function has two-step decay feature and includes a dip in the correlator at the low-k region spatially corresponding to long-range. This is considered to be indicative of the effect of interionic interactions on spatial density−density fluctuations.

For analyzing calculated $F_s(k,t)$ and $F_{coh}(k,t)$ values, we employ a modified-type Kohlraush−Williams−Watts (KWW) function[85] as follows

$$F(k,t) = A\exp(-t/\tau_\beta) + (1-A)\exp[-(t/\tau_\alpha)^\beta] \quad (7)$$

where τ_α and τ_β are the relaxation times of the α and β processes, respectively, and β is the stretching parameter of the α relaxation. Also, it is assumed that the β relaxation has an exponential form and that the α relaxation has a stretched exponential form. (See the Supporting Information for the result of the fitting function.)

dx.doi.org/10.1021/jp3110425 | J. Phys. Chem. B 2013, 117, 1136−1150

Figure 13a,b shows the estimated relaxation time, τ_β, and the stretching parameter, β, with eq 7, as a function of k. As seen in

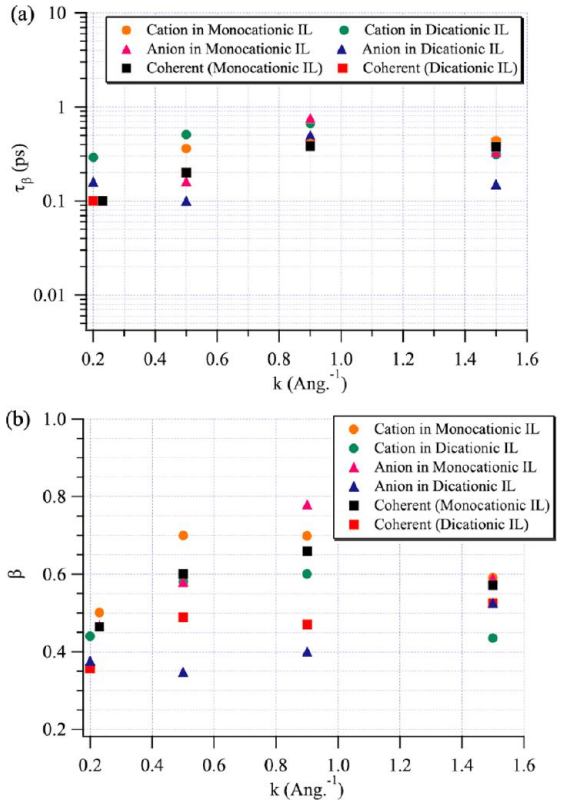

Figure 13. Fit parameter as a function of wavenumber, k: (a) structural relaxation time, τ_β, and (b) stretching parameter, β, as a function of wave vector, k.

the figures, the values of β hardly depend on k around the value of 0.55, and all the computed values of the τ_β result to be less than 1 ps. Since the β process is a fast relaxation process and is related to the spatial range where the Gaussian approximation works well,[79] the KWW function we employed is not enough to capture the β process more correctly. Therefore, we will focus on the slower decay, the α relaxation, below.

Figure 14a,b indicates the computed α relaxation time for the incoherent scattering function, τ_α (τ_{inc}), as a function of k. It is found that the k dependence of the τ_α is different between the monocation and the dication and for the anion in both the monocationic and dicationic ILs. The behavior of the k dependence for the dication is clearly distinctive compared with that for the monocation, while the anion shows similar features in both the ILs. The k value of 0.90 Å^{-1} corresponding to the maximum value of the τ_α coincides with each other, except for the case of the dication. Also, for the monocationic IL, this k value agrees with the first peak position in the $S(k)$ of the monocationic IL (see Figure 9). On the other hand, for the dicationic IL, the k value for the maximum τ_α for the dication accords with the low-k peak position (at k = 0.20 Å^{-1}) in the $S(k)$ of the dicationic IL (see Figure 9), but that for the anion in the dicationic IL corresponds to the first peak position (at k = 0.90 Å^{-1}), similar to the case of the cation and anion of the monocationic IL. Since these results are for self-motions, it is required to examine collective dynamical feature and relaxation behavior. In Figure 14c, the relaxation time of the coherent intermediate scattering function τ_{coh}, as a function of k, is displayed for the monocationic

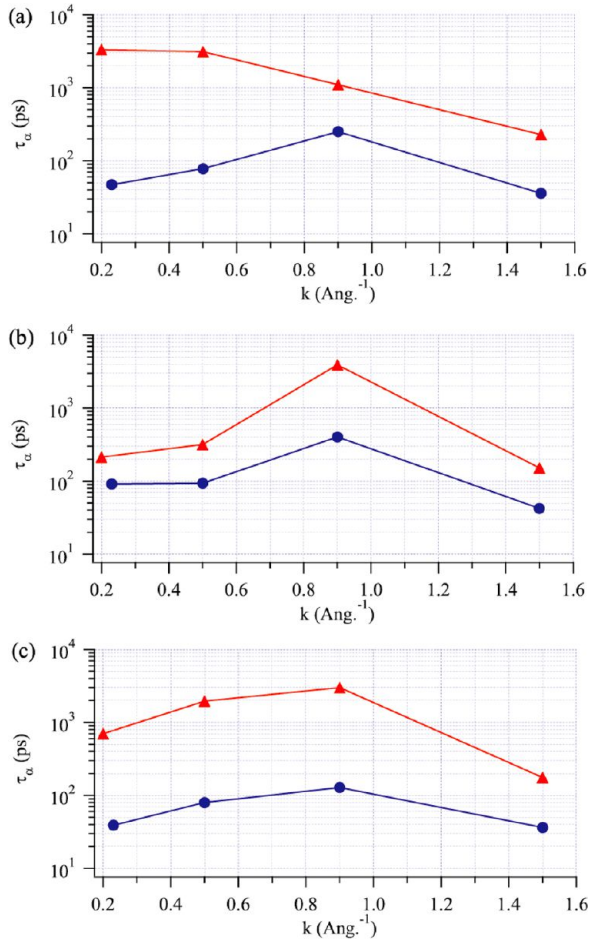

Figure 14. α relaxation time τ_α as a function of wavenumber k for (a) cation, (b) anion, and (c) coherent scattering ([C_3MIm][NTf_2], blue; [C_6(MIm)$_2$][NTf_2]$_2$, red).

and dicationic ILs, respectively. It is seen that the k value for the maximum τ_{coh} (at k = 0.90 Å^{-1}) accords with each other for both the ILs. In the analysis of the coherent intermediate scattering, our results indicate that slowing down of collective motions including cation and anion motions could occur at around the first peak (k = 0.90 Å^{-1}), corresponding to the so-called de Gennes narrowing,[79,86] while the results of incoherent characteristic times (self-motions of ions) do not show. Therefore, the correlation between self- and collective motions is examined further, next.

To investigate the relation between the τ_{coh} and the τ_{inc}, further, we consider the average relaxation time, $\langle\tau\rangle$, which represents the first moment of the equivalent distribution of relaxation times. The average relaxation time for incoherent and coherent characteristic times can be obtained for the case of KWW functions as[87,88]

$$\langle\tau\rangle = \Gamma\left(\frac{1}{\beta}\right)\frac{\tau_\alpha}{\beta} \tag{8}$$

where Γ is the Gamma function. The ratio between the coherent and incoherent average times represents to what degree self-motions correlate with collective motions. The results of the ratio are shown as a function of k with the $S(k)$ results for corresponding k ranges in Figure 15a,b. According to the de Gennes narrowing,[86] in the case of simple monatomic liquids, the coherent characteristic time is correlated with the incoherent

dx.doi.org/10.1021/jp3110425 | J. Phys. Chem. B 2013, 117, 1136−1150

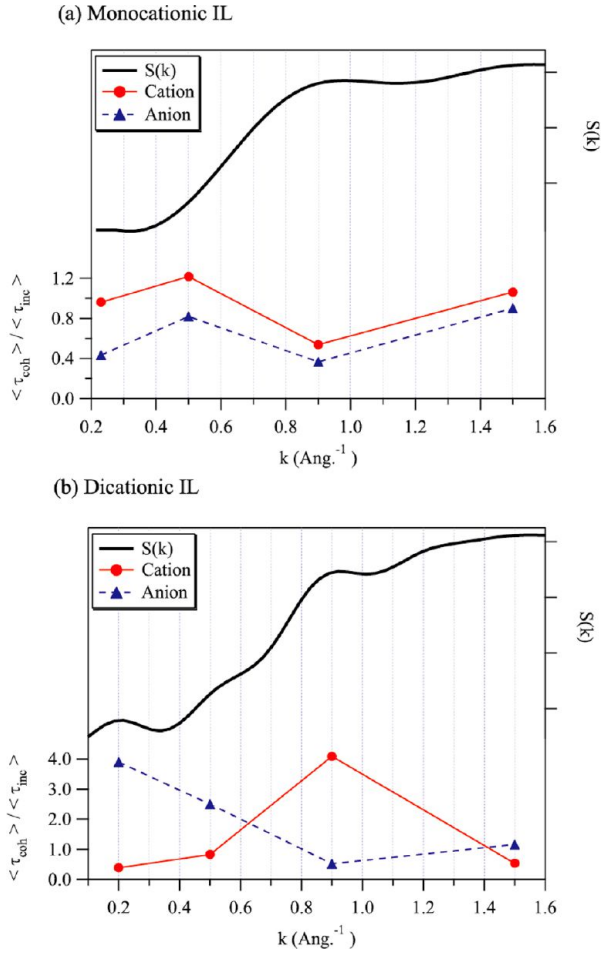

Figure 15. The ratios between the average times of τ_α corresponding to coherent and incoherent scatterings as a function of wavenumber, $\langle\tau_{coh}\rangle/\langle\tau_{inc}\rangle_{cation}$ and $\langle\tau_{coh}\rangle/\langle\tau_{inc}\rangle_{anion}$: (a) monocationic IL ($[C_3MIm][NTf_2]$) and (b) dicationic IL ($[C_6(MIm)_2][NTf_2]_2$). Each thick line shows the structure factor of the corresponding IL.

characteristic time via the $S(k)$, that is, $\langle\tau_{coh}(k)\rangle \propto S(k)\langle\tau_{inc}(k)\rangle$.[88,89] However, it is obviously seen that our current results show a deviation from the de Gennes narrowing-like relationship mentioned above. For the monocationic IL, the value of the ratio for both the cation and the anion indicates similar variation to the profile of the corresponding $S(k)$, though clear discrepancies are seen at around the first peak of the $S(k)$ (k = 0.90 Å^{-1}). These features are consistent with the previous report that, below the first maximum of $S(k)$, the behavior of the ratio strongly deviates from the de Gennes-like relationship.[88] On the basis of our results, calculated results are considered to imply that the self-motions of both the cation and the anion contribute to collective motions almost in a similar way independent of the k range. On the other hand, for the dicationic IL, we can observe the distinctive behavior of the ratio. It is found that the ratio for the anion contributes in a different way from that for the cation. From our results, the anion motion mainly influences the collective motion at around the low-k peak of the corresponding $S(k)$ (k = 0.20 Å^{-1}), while the cation motion at around the first peak of the dicationic IL does not. For the first peak position (k = 0.90 Å^{-1}), it is considered that the contribution of the cation motion to the collective motion becomes larger than that of the anion motion. Therefore, these results qualitatively indicate that, in the dicationic IL, dynamical heterogeneous behavior strongly correlates with structural variations or heterogeneity.

As discussed above, there are several aspects that are accessible to us. First is that current results derived from the consideration of dynamical properties are consistent with the suggestion, as has been examined experimentally,[47] that the appearance of a low-k peak in $[C_nMIm][NTf_2]$ ($n \leq 10$) can be mainly attributed to anion−cation, anion−anion, and cation−cation correlations, except among alkyl groups. In particular, from our analyses of the low-k peak in the $S(k)$ of the dicationic IL, the contribution of cation−anion and anion−anion correlations to the low-k peak is larger than the cation−cation correlation. As the second aspect, not only the length of an alkyl chain or a linkage chain but also the difference of charge number between the monocation and the dication influences interionic correlations.

4. CONCLUDING REMARKS

We have performed detailed theoretical investigations of dynamical properties of the monocationic IL, $[C_3MIm][NTf_2]$, and the dicationic IL, $[C_6(MIm)_2][NTf_2]_2$, employing MD simulations. On the basis of the computed VDOS results, we have considered the environment around the cation and the anion species and have carried out comparative studies of dynamical behavior due to the relaxation process with the calculated Kerr spectra. It has been observed that the computed Kerr spectra are qualitatively in good accord with the experimental results. For the monocationic IL, we have found that the contribution of cation−anion cross-correlations to the total Kerr profile is predominant at the frequency region lower than 50 cm^{-1}, while both the cation and the cross-correlation components contribute almost equivalently at the higher frequency region than 50 cm^{-1}. In contrast, the computed Kerr profile of the dicationic IL showed the characteristic peak at between 50 and 100 cm^{-1}, which did not appear in the Kerr spectrum of the monocationic IL. We have investigated this difference in the spectra further, considering the interaction-induced effect on ion dynamics and the reorientational motions of ion molecules. It has been found that the reorientational motions of ions mainly contribute to the Kerr spectrum profile.

For studying the contribution of characteristic reorientational (librational) motion such as libration motion, the analysis of librational dynamics has been carried out. From the results obtained with the model of Gaussian-distributed oscillators, we have shown that the difference of the Kerr spectra in between the monocationic and dicationic ILs could be mainly ascribed to the distinctive angular momentum of the monocation, $[C_3MIm]^+$, and the dication, $[C_6(MIm)_2]^{2+}$, depending on its librational motion about a specified body-fixed coordinate axis. Also, it has been found out that the contribution of anion motions, through interionic interactions with counter cations, could be observable at the frequency region of less than 50 cm^{-1}. In contrast to the cations, the librational dynamics of the anion, $[NTf_2]^-$, indicated remarkably characteristic features, which are quite similar to each other in both the monocationic and dicationic ILs, including a common sharp peak as shown in the autocorrelator of angular momentum. Also, it has been indicated that peak intensities at the frequencies lower than 50 cm^{-1} are much larger than at the following frequencies, except for the sharp peaks. Therefore, it has been shown that the dominant contribution of the anion to the total Kerr profiles is due to low-frequency modes (<50 cm^{-1}) coming from librational motion of the anion, as previously pointed out. In addition, it has been shown that a sharp peak at around 90 cm^{-1} appears in both the ILs and that this sharp peak

dx.doi.org/10.1021/jp3110425 | J. Phys. Chem. B 2013, 117, 1136−1150

corresponds to an intermolecular motion coupled to a peak frequency mode with relatively large Raman activity predicted with quantum chemical calculation result of the anion.

Furthermore, from the investigation of collective dynamics of ILs with the MSD, the non-Gaussian parameter, and the incoherent and coherent intermediate scattering functions, we have found that the analysis of the spatial dynamics of the anion indicates the rattling motion of the anion inside the cage formed in each IL. Thereby, it has been found that the difference of relaxation behavior (non-Gaussian behavior) between the monocation and the dication influences the distinction of the Kerr spectra between the monocationic and dicationic ILs.

The total X-ray structure factors for both the monocationic and dicationic ILs were calculated, and it has been found that some of characteristic peaks are included consistent with the experimental results of other IL systems. In particular, the low-k peak at 0.20 $Å^{-1}$ appeared for the dicationic IL, while we did not see it for the monocationic IL. In addition, we have analyzed a two-step relaxation feature in the computed intermediate scattering functions with a modified KWW function. With the calculated ratio between the incoherent and coherent average relaxation time, it has been found that, different from simple monatomic liquids, both the ILs show obvious deviation from the de Gennes narrowing-like relationship. Also, we observed the distinctive behavior of the ratio for the dicationic IL, while the value of the ratio showed similar variation for both the monocation and the anion in the monocationic IL. Thus, it is suggested that, in the monocationic IL, the self-motions of both the cation and the anion contribute to collective motions in almost a similar way, independent of the k range. On the other hand, it is considered that, in the dicationic IL, the ratio for the anion contributes in a different way from that for the dication and that the anion motion mainly influences the collective motion at around the low-k peak of the corresponding $S(k)$, while the cation motion does so at around the first peak of the dicationic IL. Therefore, it is suggested that, in the dicationic IL, dynamical heterogeneous behavior strongly correlates with structural variations or heterogeneity.

Current studies suggest that the appearance of the low-k peak in the dicationic IL can be mainly attributed to anion−cation, anion−anion, and cation−cation correlations, except among the alkyl groups, consistent with the suggestion of the molecular-level origin of low-k peak in $[C_nMIm][NTf_2]$ ($n \leq 10$) IL from experimental data.[47] In particular, the contribution of the cation−anion and anion−anion correlations to the low-k peak is more significant than the cation−cation correlation. Also, both the length of an alkyl chain or a linkage chain and the difference of charge number between the monocation and the dication influence interionic correlations.

APPENDIX: CALCULATIONS OF POLARIZABILITY TIME CORRELATION FUNCTIONS AND KERR SPECTRA

The total polarizability of the system, $\Pi(t)$, is represented as the sum of the molecular polarizability part (denoted as M), $\Pi^{M}(t) = \sum_{i=1}^{N}\alpha_i(t)$, where N is the number of molecules and α_i denotes the polarizability tensor of molecule i, and the interaction-induced polarizability (denoted as II), $\Pi^{II}(t)$, as follows

$$\Pi(t) = \Pi^{M}(t) + \Pi^{II}(t) \tag{9}$$

where t indicates the time dependence. The interaction-induced polarizability in the dipole-induced-dipole (DID) model approximation[64,90] is represented as follows

$$\Pi^{II}(t) = \sum_{i=1}^{N}\sum_{j\neq i}^{N}\alpha_i(t)\, T_{ij}(t)\, \tilde{\alpha}_j(t) \tag{10}$$

where T_{ij} means the dipole interaction tensor between molecules i and j. $\tilde{\alpha}_i(t)$ is the effective polarizability for molecule i defined by the following equation including the interaction-induced effects

$$\tilde{\alpha}_i(t) = \alpha_i(t) + \sum_{j\neq i}^{N}\alpha_i(t)\, T_{ij}(t)\, \tilde{\alpha}_j(t) \tag{11}$$

The time correlation function of the off-diagonal elements of the total polarizability, ϕ, can be defined as $\phi(t) = \langle \mathrm{Tr}(\beta(0)\,\beta(t))\rangle$ where β represents the anisotropic component of the total polarizability, Π. When $\beta = \beta^{M} + \beta^{II}$, $\phi(t)$ can be separated into three parts, $\phi(t) = \phi^{mol}(t) + \phi^{ind}(t) + \phi^{cross}(t)$, where ϕ^{mol}, ϕ^{ind}, and ϕ^{cross} are a molecular part, an interaction-induced part, and a molecular-interaction-induced cross-correlation part, respectively. Also, in the case in which $\beta = \beta^{C} + \beta^{A}$, where C and A denote the cationic and anionic anisotropic components of the total polarizability, $\Pi = \Pi^{C} + \Pi^{A}$, $\phi(t)$ can be decomposed into three parts, $\phi(t) = \phi^{C}(t) + \phi^{A}(t) + \phi^{C-A}(t)$, where ϕ^{C}, ϕ^{A}, and ϕ^{C-A} are the cation contribution, the anion contribution, and the cation−anion cross-correlation contribution, respectively. For the more detailed expression of each component of the ϕ, readers should refer to references previously reported.[14,41]

To investigate dynamics such as reorientational motion, the projection scheme to separate the reorientational part (denoted as R) from the collision-induced part (denoted as CI) as proposed in previous works[64,65] is employed to rewrite the $\beta = \beta^{M} + \beta^{II}$ part as

$$\begin{aligned}\beta^{M}(t) + \beta^{II}(t) &= (1+f)\beta^{M}(t) + (\beta^{II}(t) - f\beta^{M}(t)) \\ &= \beta^{R}(t) + \beta^{CI}(t)\end{aligned} \tag{12}$$

where the projection factor, f, is defined as

$$f = \frac{\mathrm{Tr}(\beta^{\Pi}\beta^{M})}{\mathrm{Tr}(\beta^{M}\beta^{M})} \tag{13}$$

and then the $\phi(t)$ can be separated into three parts,[14,41] $\phi(t) = \phi^{R}(t) + \phi^{CI}(t) + \phi^{R-CI}(t)$, where ϕ^{R}, ϕ^{CI}, and ϕ^{R-CI} are the reorientational part, the collision-induced part, and the reorientational-collision-induced part, respectively.

The Kerr profile is obtained by the Fourier transform of the time derivative of the $\phi(t)$ as follows

$$R(\omega) = 2\frac{1 - e^{-\hbar\omega/k_B T}}{1 + e^{-\hbar\omega/k_B T}}\int_0^{\infty}\sin(\omega t)\, R(t)\, dt \tag{14}$$

where $\hbar = h/2\pi$, and h is the Planck constant. k_B is the Boltzmann constant. Therefore, the Kerr signal in the frequency domain can be represented as $R(\omega) = R^{mol}(\omega) + R^{ind}(\omega) + R^{cross}(\omega)$, $R(\omega) = R^{C}(\omega) + R^{A}(\omega) + R^{C\text{-}A}(\omega)$, and $R(\omega) = R^{R}(\omega) + R^{CI}(\omega) + R^{R\text{-}CI}(\omega)$, respectively.

For the computation of the molecular polarizability, eq 11 was solved iteratively under the all-orders DID approximation.[91] Also, to avoid the unphysical divergence of the polarization[92] in the computation of dipole interaction tensors, we employed the Thole's model.[92] In our calculation, we considered the distance

and vector between the centers of mass of distinct molecules in the dipole interaction tensor. Therefore, the range of the attenuation of dip[10]polar interactions at short distances, s, was computed with the definition[92] $s = 1.662(A_iA_j)^{1/6}$, where A_i and A_j denote the molecular polarizabilities set at the centers of mass of molecules i and j, respectively. It should be noted that, only in evaluating the range of attenuation of dipolar interactions, both the A_i and the A_j were taken as isotropic and scalar in our model and that, for the molecular polarizabilities, A_i and A_j, we used 12.607 Å^3 for $[C_3MIm]^+$, 25.472 Å^3 for $[C_6(MIm)_2]^{2+}$, and 11.259 Å^3 for $[NTf_2]^-$, from the ab initio calculations.[58]

■ ASSOCIATED CONTENT

Supporting Information

Additional information (fit parameters, $\beta(t) = d[\log(MSD)]/d[\log(t)]$, computed partial structure factors for the dicationic IL, and intermediate scattering function with the result of fitting function) as noted in text. This material is available free of charge via the Internet at http://pubs.acs.org.

■ AUTHOR INFORMATION

Corresponding Author

*E-mail: ishida@ims.ac.jp (T.I.), shirota@faculty.chiba-u.jp (H.S.).

Notes

The authors declare no competing financial interest.

■ ACKNOWLEDGMENTS

T.I. gratefully acknowledges research support by the Ministry of Education, Culture, Sports, Science and Technology (MEXT) of Japan (Grant in Aid for Scientific Research (C): 23550029). H.S. is grateful for support of this research by the Ministry of Education, Culture, Sports, Science and Technology (MEXT) of Japan (Grant in Aid for Young Scientists (A): 21685001) and the Iwatani Naoji Foundation.

■ REFERENCES

(1) *Ionic Liquids in Synthesis*, 2nd ed.; Wasserscheid, P., Welton, T., Eds.; Wiley-VCH: Weinheim, 2008.
(2) *Electrochemical Aspects of Ionic Liquids*; Ohno, H., Ed.; Wiley-Interscience: Hoboken, NJ, 2005.
(3) Rogers, R. D.; Voth, G. A. Special Issue on Ionic Liquids. *Acc. Chem. Res.* **2007**, *40* (11), 1077−1236.
(4) Weingaertner, H. *Angew. Chem., Int. Ed.* **2008**, *47*, 654−670.
(5) *Ionic Liquids: Theory, Properties, New Approaches*; Kokorin, A., Ed.; InTech: Rijeka, Croatia, 2011.
(6) Castner, E. W., Jr.; Wishart, J. F. *J. Chem. Phys.* **2010**, *132*, 120901/1−9.
(7) Seddon, K. R. *J. Chem. Technol. Biotechnol.* **1997**, *68*, 351−356.
(8) Welton, T. *Chem. Rev.* **1999**, *99*, 2071−2084.
(9) Wishart, J. F. *Energy Environ. Sci.* **2009**, *2*, 956−961.
(10) Baldelli, S. *Acc. Chem. Res.* **2008**, *41*, 421−431.
(11) Maginn, E. J. *Acc. Chem. Res.* **2007**, *40*, 1200−1207.
(12) Shirota, H.; Fukazawa, H. Atom Substitution Effects in Ionic Liquids: A Microscopic View by Femtosecond Raman-Induced Kerr Effect Spectroscopy. In *Ionic Liquids: Theory, Properties, New Approaches*; Kokorin, A., Ed.; InTech: Rijeka, Croatia, 2011; pp 201−224.
(13) Shirota, H.; Nishikawa, K.; Ishida, T. *J. Phys. Chem. B* **2009**, *113*, 9831−9839.
(14) Ishida, T.; Nishikawa, K.; Shirota, H. *J. Phys. Chem. B* **2009**, *113*, 9840−9851.
(15) Ishida, T. The Unique Physical and Chemical Properties of Ionic Liquids through Interionic Interactions: Theoretical Investigation with Molecular Dynamics Simulations. In *Handbook of Ionic Liquids: Properties, Applications and Hazards*; Mun, J., Sim, H., Eds.; Nova Scientific Publishers: Hauppauge, NY, 2012; pp 395−417.
(16) Shirota, H. *ChemPhysChem* **2012**, *13*, 1638−1648.
(17) Castner, E. W., Jr.; Wishart, J. F.; Shirota, H. *Acc. Chem. Res.* **2007**, *40*, 1217−1227.
(18) Castner, E. W., Jr.; Margulis, C. J.; Maroncelli, M.; Wishart, J. F. *Annu. Rev. Phys. Chem.* **2011**, *62*, 85−105.
(19) Bhargava, B. L.; Balasubramanian, S.; Klein, M. L. *Chem. Commun.* **2008**, 3339−3351.
(20) Maginn, E. J. *J. Phys.: Condens. Matter* **2009**, *21*, 373101/1−17.
(21) Shim, Y.; Jeong, D.; Manjari, S.; Choi, M. Y.; Kim, H. J. *Acc. Chem. Res.* **2007**, *40*, 1130−1137.
(22) Lall, S. I.; Mancheno, D.; Castro, S. B.; Cohen, J. I.; Engel, R. *Chem. Commun.* **2000**, 2413−2414.
(23) Engel, R.; Cohen, J. I.; Lall, S. I. *Phosphorus, Sulfur Silicon Relat. Elem.* **2000**, *177*, 1441−1445.
(24) Lall, S.; Behaj, V.; Mancheno, D.; Casiano, R.; Thomas, M.; Rikin, A.; Gaillard, J.; Raju, R.; Scumpia, A.; Castro, S.; et al. *Synthesis* **2002**, 1530−1540.
(25) Engel, R.; Cohen, J. I. *Curr. Org. Chem* **2002**, *6*, 1453−1467.
(26) Wishart, J. F.; Lall-Ramnarine, S. I.; Raju, R.; Scumpia, A.; Bellevue, S.; Ragbir, R.; Engel, R. *Radiat. Phys. Chem.* **2005**, *72*, 99−104.
(27) Yoshizawa, M.; Ito-Akita, K.; Ohno, H. *Electrochim. Acta* **2000**, *45*, 1617−1621.
(28) Ito, K.; Nishina, N.; Ohno, H. *Electrochim. Acta* **2000**, *45*, 1295−1298.
(29) Anderson, J. L.; Ding, R.; Ellern, A.; Armstrong, D. W. *J. Am. Chem. Soc.* **2005**, *127*, 593−604.
(30) Shirota, H.; Mandai, T.; Fukazawa, H.; Kato, T. *J. Chem. Eng. Data* **2011**, *56*, 2453−2459.
(31) Sun, H.; Zhang, D.; Liu, C.; Zhang, C. *J. Mol. Struct. THEOCHEM* **2009**, *900*, 37−43.
(32) Bodo, E.; Caminiti, R. *J. Phys. Chem. A* **2010**, *114*, 12506−12512.
(33) Bhargava, B. L.; Klein, M. L. *J. Chem. Theory Comput.* **2010**, *6*, 873−879.
(34) Bodo, E.; Chiricotto, M.; Caminiti, R. *J. Phys. Chem. B* **2011**, *115*, 14341−14347.
(35) Yeganegi, S.; Soltanabadi, A.; Farmanzadeh, D. *J. Phys. Chem. B* **2012**, *116*, 11517−11526.
(36) Shirota, H.; Ishida, T. *J. Phys. Chem. B* **2011**, *115*, 10860−10870.
(37) Widmer-Cooper, A.; Harrowell, P.; Fynewever, H. *Phys. Rev. Lett.* **2004**, *93*, 135701/1−4.
(38) Yang, P.; Voth, G. A.; Xiao, D.; Hines, L. G., Jr.; Bartsch, R. A.; Quitevis, E. L. *J. Chem. Phys.* **2011**, *135*, 034502/1−12.
(39) Giraud, G.; Gordon, C. M.; Dunkin, I. R.; Wynne, K. *J. Chem. Phys.* **2003**, *119*, 464−477.
(40) Urahata, S. M.; Ribeiro, M. C. C. *J. Chem. Phys.* **2005**, *122*, 024511/1−9.
(41) Hu, Z.; Huang, X.; Annapureddy, H. V. R.; Margulis, C. J. *J. Phys. Chem. B* **2008**, *112*, 7837−7849.
(42) Shirota, H.; Castner, E. W., Jr. *J. Phys. Chem. A* **2005**, *109*, 9388−9392.
(43) Bardak, F.; Xiao, D.; Hines, L. G., Jr.; Son, P.; Bartsch, R. A.; Quitevis, E. L.; Yang, P.; Voth, G. A. *ChemPhysChem* **2012**, *13*, 1687−1700.
(44) Triolo, A.; Russina, O.; Fazio, B.; Triolo, R.; Cola, E. D. *Chem. Phys. Lett.* **2008**, *457*, 362−365.
(45) Triolo, A.; Russina, O.; Bleif, H.-J.; Di Cola, E. *J. Phys. Chem. B* **2007**, *111*, 4641−4644.
(46) Russina, O.; Triolo, A.; Gontrani, L.; Caminiti, R.; Xiao, D.; Hines, J. L. G.; Bartsch, R. A.; Quitevis, E. L.; Plechkova, N.; Seddon, K. R. *J. Phys.: Condens. Matter* **2009**, *21*, 424121/1−9.
(47) Fujii, K.; Kanzaki, R.; Takamuku, T.; Kameda, Y.; Kohara, S.; Kanakubo, M.; Shibayama, M.; Ishiguro, S.; Umebayashi, Y. *J. Chem. Phys.* **2011**, *135*, 244502/1−11.
(48) Bhargava, B. L.; Klein, M. L.; Balasubramanian, S. *ChemPhysChem* **2008**, *9*, 67−70.
(49) Sarangi, S. S.; Zhao, W.; Müller-Plathe, F.; Balasubramanian, S. *ChemPhysChem* **2010**, *11*, 2001−2010.

(50) Annapureddy, H. V. R.; Kashyap, H. K.; De Biase, P. M.; Margulis, C. J. *J. Phys. Chem. B* **2010**, *114*, 16838−16846.
(51) Santos, C. S.; Annapureddy, H. V. R.; Murthy, N. S.; Kashyap, H. K.; Castner, E. W., Jr.; Margulis, C. J. *J. Chem. Phys.* **2011**, *134*, 064501/1−10.
(52) Smith, W.; Forster, T. R. *The DL_POLY_2 User Manual*; Daresbury Laboratory: Daresbury, United Kingdom, 2001.
(53) Lopes, J. N. C.; Deschamps, J.; Padua, A. A. H. *J. Phys. Chem. B* **2004**, *108*, 2038−2047.
(54) Lopes, J. N. C.; Deschamps, J.; Padua, A. A. H. *J. Phys. Chem. B* **2004**, *108*, 11250.
(55) Köddermann, T.; Paschek, D.; Ludwig, R. *ChemPhysChem* **2007**, *8*, 2464−2470.
(56) Allen, M. P.; Tildesley, D. J. *Computer Simulation of Liquids*; Oxford: Clarendon, 1987.
(57) Smith, W. *Comput. Phys. Commun.* **1992**, *67*, 392−406.
(58) Frisch, M. J.; Trucks, G. W.; Schlegel, H. B.; Scuseria, G. E.; Robb, M. A.; Cheeseman, J. R.; Montgomery, J. A., Jr.; Vreven, T.; Kudin, K. N.; Burant, J. C.; et al. *GAUSSIAN 03*; Gaussian, Inc.: Pittsburgh, PA, 2003.
(59) Becke, A. D. *J. Chem. Phys.* **1993**, *98*, 5648−5652.
(60) Lee, C.; Yang, W.; Parr, R. G. *Phys. Rev. B* **1988**, *37*, 785−589.
(61) Dunning, T. H., Jr. *J. Chem. Phys.* **1989**, *90*, 1007−1023.
(62) Woon, D. E.; Dunning, T. H., Jr. *J. Chem. Phys.* **1993**, *98*, 1358−1371.
(63) Liu, H.; Maginn, E. *J. Chem. Phys.* **2011**, *135*, 124507/1−16.
(64) Frenkel, D.; McTague, J. P. *J. Chem. Phys.* **1980**, *72*, 2801−2818.
(65) Stassen, H.; Dorfmüller, T.; Ladanyi, B. M. *J. Chem. Phys.* **1994**, *100*, 6318−6330.
(66) Lynden-Bell, R. M.; Steele, W. A. *J. Phys. Chem.* **1984**, *88*, 6514−6518.
(67) Chelli, R.; Cardini, G.; Procacci, P.; Righini, R.; Califano, S. *J. Chem. Phys.* **2000**, *113*, 6851−6863.
(68) Chelli, R.; Cardini, G.; Procacci, P.; Righini, R.; Califano, S. *J. Chem. Phys.* **2002**, *116*, 6205−6215.
(69) Fukazawa, H.; Ishida, T.; Shirota, H. *J. Phys. Chem. B* **2011**, *115*, 4621−4631.
(70) Landau, L. D.; Lifshitz, E. M. *Machanics*, 3rd ed. ed.; Butterworth-Heinemann: Oxford, 1982.
(71) Goldstein, H.; Poole, C.; Safko, J. *Classical Mechanics*, 3rd ed.; Pearson Education, Inc.: San Francisco, 2002.
(72) Fujisawa, T.; Nishikawa, K.; Shirota, H. *J. Chem. Phys.* **2009**, *131*, 244519/1−14.
(73) Kendall, R. A.; Dunning, T. H., Jr.; Harrison, R. J. *J. Chem. Phys.* **1992**, *96*, 6796−6806.
(74) Rahman, A. *Phys. Rev.* **1964**, *136*, A405−A411.
(75) Del Pópolo, M. G.; Voth, G. A. *J. Phys. Chem. B* **2004**, *108*, 1744−1752.
(76) Colmenero, J.; Alvarez, F.; Arbe, A. *Phys. Rev. E* **2002**, *65*, 041804/1−12.
(77) *International Tables for Crystallography, Vol. C*; Prince, E., Ed.; International Union of Crystallography: Chester, England, 2006.
(78) To improve and verify the resolution of frequency domain, we employed zero-padding for the pair correlation function prior to taking its Fourier transform.
(79) Balucani, U.; Zoppi, M. *Dynamics of the Liquid State*; Clarendon Press: Oxford, UK, 1994.
(80) Ngai, K. L. *Relaxation and Diffusion in Complex Systems*; Springer: New York, 2011.
(81) Götze, W. *Complex Dynamics of Glass-Forming Liquids, a Mode-Coupling Theory*; Oxford University Press Inc.: New York, 2009.
(82) Berthier, L.; Biroli, G.; Bouchaud, J.-P.; Cipelletti, L.; van Saarloos, W. *Dynamical Heterogeneities in Glasses, Colloids and Granular Media*; Oxford University Press Inc.: New York, 2011.
(83) Jarosz, G.; Mierzwa, M.; Ziozo, J.; Paluch, M.; Shirota, H.; Ngai, K. L. *J. Phys. Chem. B* **2011**, *115*, 12709−12716.
(84) Horbach, J.; Kob, W. *Phys. Rev. E* **2001**, *64*, 041503/1−14.
(85) Qiu, X.; Moe, N. E.; Ediger, M. D.; Fetters, L. J. *J. Chem. Phys.* **2000**, *113*, 2918−2926.
(86) de Gennes, P. G. *Physica* **1959**, *25*, 825−839.
(87) Müller-Plathe, F.; van Gunsteren, W. F. *J. Chem. Phys.* **1995**, *103*, 4745−4756.
(88) Arbe, A.; Colmenero, J. *Phys. Rev. E* **2009**, *80*, 041805/1−13.
(89) Zorn, R.; Arbe, A.; Colmenero, J.; Frick, B.; Richter, D.; Buchenau, U. *Phys. Rev. E* **1995**, *52*, 781−795.
(90) Geiger, L. C.; Ladanyi, B. M. *J. Chem. Phys.* **1987**, *87*, 191−202.
(91) Kiyohara, K.; Kamada, K.; Ohta, K. *J. Chem. Phys.* **2000**, *112*, 6338−6348.
(92) Thole, B. T. *Chem. Phys.* **1981**, *59*, 341−350.